Adsorption of Camphor on Au(111) and Its Effect on the Electroreduction of Periodate (IO_4^-)†

Matthias Danckwerts,*,‡,§ Yong-Jun Li,‡ Julia Oslonovitch,‡ Bruno Pettinger,‡ and Katharina Krischer‡,||

Fritz-Haber-Institut der Max-Planck-Gesellschaft, Faradayweg 4-6, 14195 Berlin, Germany, and Physics Department E19, Technische Universität München, James-Franck-Strasse 1, 85748 München, Germany

Received: January 7, 2004; In Final Form: April 21, 2004

The potential-controlled physisorption of camphor on Au(111) single-crystalline bulk as well as thin film electrodes and its influence on the electroreduction of IO_4^- to IO_3^- is studied. Besides cyclic voltammetry (CV), we use second-harmonic generation (SHG) to study electronic and structural properties of the surface and surface-plasmon resonance (SPR) shift measurements to probe the interfacial dielectric function, which is influenced by adsorption. Emphasis is placed on the interplay of surface reconstruction with the adsorption of neutral and ionic species and the reaction dynamics. Independent of the presence of the electroactive species IO_4^-, a 2D-condensed layer of camphor forms in a certain potential range and tends to preserve the structure of the surface. The film inhibits the electroreduction of IO_4^- at negative potentials and is displaced from the surface by periodate-derived anions at more positive potentials, whereupon the reaction is resumed. The anion adsorption causes a fast lifting of the reconstruction which is not fully restored on the reversed potential sweep owing to the re-formation of the condensed camphor film.

1. Introduction

In electrochemistry, the adsorption of organic species on metal electrodes receives unbroken attention due to both fundamental and technical interest. One of the reasons is the ability of many organic films to inhibit electron-transfer reactions. The effect is exploited in corrosion protection technology but also has considerable implications for electrocatalysis, where organic contaminants or reaction intermediates may reduce the surface activity considerably. Basic considerations to understand and control this behavior concern the process of electron tunneling across the film and the influence of an organic adsorbate layer on the potential distribution at the surface, as well as the origin of the inhibiting effect, which may be associated with the electron transition probability and changes in the activation energy of the transfer reaction.

It was found recently that the electroreduction of periodate on Au(111) is blocked by camphor adsorbing on the surface.[1] This system is interesting not just as a model for reaction inhibition on a well-defined single-crystal surface. In particular, the interplay of camphor and periodate under the influence of the electrode potential constitutes an activator-inhibitor system exhibiting nonlinear spatiotemporal reaction dynamics. This leads to the formation of stationary Turing-type patterns on the electrode surface.[1] These patterns were observed using surface-plasmon resonance imaging.

Organic film formation is influenced by the surface structure of the electrode. As an example, the adsorption of pyridine strongly depends on the crystal structure.[2,3] In ref 4, the 2D-condensation of uracil and uridine on vicinal Au(111) surfaces is found to be perturbed by steps; a flat surface seems to be a prerequisite for the formation of a 2D condensed film. The dissolution kinetics of uridine adlayers on Au single crystal electrodes, probed by potential-step voltammetry, is also strongly influenced by steps.[5] The authors conclude that on vicinal surfaces the ordering of the organic film is significantly disturbed. Furthermore, by scanning-tunneling microscopy (STM), it was found that physisorbed uracil adlayers on Au(100) undergo lateral restructuring following the substrate surface (hex) → (1 × 1) transition.[6] For camphor and its derivatives, Striegler et al. give a survey of organic adsorption on reconstructed and (1 × 1) Au low index surfaces.[7,8] The dependence of adsorption and 2D condensation on substrate orientation and structure is investigated by means of cyclic voltammetry and measurements of the differential capacity of the double layer. As a direct approach to measure changes in the surface structure in such systems, we reported on SHG anisotropy studies of the interplay between camphor condensed-film formation and the formation or lifting of the ($\sqrt{3} \times 23$) surface reconstruction of a Au(111) electrode.[9]

In this paper, we extend these studies to a situation where, in addition, an electroactive species is present. We investigate the correlation of the electrochemical reactivity of Au(111) in electrolytes containing periodate and camphor with structural parameters of the crystal surface. The complex dynamics of reaction kinetics and mass transport in this system is investigated in ref 1 and further work.[10,11] Here, we demonstrate the interaction between surface structure, condensation of organic 2D films, and the reactivity of the interface. In combination with cyclic voltammetry, we use second-harmonic generation (SHG) anisotropy analysis and measurements of the surface plasmon resonance shift to obtain information on adsorbed species. Relating SHG directly to the current−voltage data became possible by applying a new scan-mode method, which

* Corresponding author. Fax: +49-30-838-56059.E-mail: matthias.danckwerts@physik.fu-berlin.de.

† Part of the special issue "Gerhard Ertl Festschrift".

‡ Fritz-Haber-Institut der Max-Planck-Gesellschaft.

§ Present address: Freie Universität Berlin, Institut für Experimentalphysik, Arnimallee 14, 14195 Berlin, Germany.

|| Technische Universität München.

10.1021/jp049920k CCC: $27.50
Published on Web 07/03/2004

by sampling SHG data during multiple voltammetric sweeps at different rotational angles allows the determination of relevant SHG symmetry components. Hence, the combination of the employed methods enabled us to follow the rate of periodate reduction and simultaneously observe structural changes of the electrode surface as well as the adsorption and desorption of ionic species and of camphor. Thus, the role of the reconstruction of the Au surface in the reaction and inhibition processes could be studied. This set of experimental in situ techniques proved very well suited for studying this complex system.

After describing experimental details in section 2, we first review two isolated subsystems that were already studied earlier,[9] namely Au(111) in $NaClO_4$ base electrolyte without and with camphor (section 3.1). Subsequently, we report results on Au(111) in $NaClO_4$ containing 10 mM $NaIO_4$ (section 3.2) and on the combined system with periodate and camphor interacting on the surface (section 3.3). Conclusions are presented in section 4.

2. Sample Preparation and Experimental Setup

Electrolytes and Sample Preparation. The electrolyte solutions were prepared from $NaIO_4$ and $NaClO_4$ salts (Sigma Aldrich, 99.8% and Merck, pA qualities, respectively) by dissolving in ultrapure water (Millipore). Two different bulk Au(111) crystals were used (both Mateck, Germany), which were cut to orientation tolerances of $<0.4°$ and $<0.5°$, respectively. To keep it clean, the crystal used in SHG experiments was stored in a 1:1 mixture of sulfuric acid and hydrogen peroxide (65%). Before an experiment, the crystal was either annealed in a hydrogen flame to light orange glow for 5 min or several times in a butane flame for a few 10 s (only data in Figure 9); after that, it was allowed to cool slowly in air before transferring into the electrochemical cell. For SPR measurements, the working electrode was a 50 nm thick gold film evaporated onto a glass plate (B270, Schott, Germany) with a 2 nm thick Cr layer beneath the gold for better adherence. The film was flame annealed in a gentle butane flame immediately before the experiment. A saturated mercury sulfate electrode (SMSE) was used as the reference electrode ($E_0 = 0.650$ V vs SHE[12]). All potentials are given with respect to this electrode.

Surface Plasmon Resonance Experiments. The optical properties of the electrode surface are probed by investigation of surface plasmon resonance (SPR) shifts. Frequency and momentum of surface plasmons depend sensitively on the dielectric constants of the interface.[13] Therefore, surface plasmon resonance measurements are a powerful tool for the characterization of electrified interfaces. In the Kretschmann configuration, light is passed through a glass prism of high refractive index whose base is in direct contact with a thin metal film; see Figure 1a. The evanescent wave created at the prism/metal/electrolyte interface during total internal reflection excites surface plasmon modes. Changing the angle of incidence α of the photons allows the wave vector of photons in the propagation direction of the plasmons $k_x = \omega/c\ n \sin \alpha$ to be varied, and thus resonance conditions can always be achieved.

In general, polarization of the interface results in slightly changed optical properties of the interface which manifest themselves in a shift of the dispersion relation of the surface plasmons. This shift is particularly pronounced when polarizable anions or organic species adsorb at the electrode surface. Thus, by following the resonance angle during a scan of the applied voltage, information about the adsorption of species is obtained.

The SPR measurements were carried out in the Kretschmann configuration with a HeNe laser. The glass plate supporting the Au thin film electrode was brought into optical contact to a glass hemisphere (BK7, Schott, Germany). The coherence of the laser light was destroyed by guiding it through a rotating sheet of scattering paper fixed between glass plates. Behind the plates a polarizer reestablished linear polarization and a $\lambda/2$-plate allowed easy switching between the s and p polarizations. With several lenses the laser beam was first widened and then focused onto the electrode. In this way, the reflected light contained the resonance curve around the minimum position which was made visible by putting a screen in the optical path of the reflected beam. The intensity profile on the screen was recorded with a single line CCD (703 E, Vistek) in which the standard 8bit ADC was exchanged by a 12bit ADC. The optical data were stored simultaneously with current and potential during a potentio-dynamic experiment. To correct for the Gaussian intensity profile and any other inhomogeneities in the laser beam, the intensity profiles obtained with p-polarized light were normalized to those obtained with s-polarization. The resulting minimum position of the resonance curve was obtained from a polynomial fit of fifth degree around the minimum. The relative angle shift could be determined with a precision of about 0.01°.

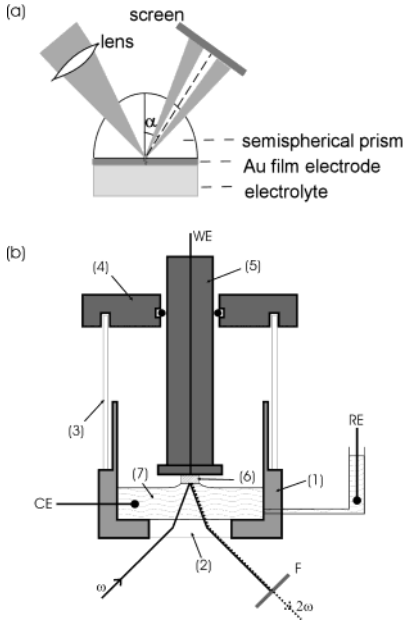

Figure 1. Experimental setups. (a) SPR Kretschmann configuration setup. (b) Electrochemical SHG cell: 1, Kel-F cell; 2, quartz glass window; 3, glass cylinder; 4, static part of steel top; 5, adjustable rotary sample holder; 6, single-crystal sample; 7, electrolyte solution. Key: WE, working electrode contact; RE, reference electrode; CE, counter electrode.

Second Harmonic Generation Measurements. Changes of surface symmetries and electric properties of the double layer are detected using SHG, where an incoming laser beam at frequency ω is converted into radiation at 2ω by nonlinear optical interaction. In dipole approximation, the rotational anisotropy of the SHG intensity at low-index fcc metal surfaces can be described as a superposition of isotropic as well as anisotropic components:

$$I_{SHG}(\varphi) \propto |\tilde{E}(2\omega, \varphi)|^2 \propto |\tilde{A} + \tilde{B}\cos(\varphi) + \tilde{C}\cos(2\varphi) + \tilde{D}\cos(3\varphi)|^2 \quad (1)$$

where $\tilde{E}(2\omega, \varphi)$ is the complex second-harmonic field and $\tilde{A}$, $\tilde{B}$, $\tilde{C}$, and $\tilde{D}$ represent the isotropic, 1-fold, 2-fold, and 3-fold symmetry coefficients, respectively. In general, these are

complex numbers, as denoted by the tilde over the symbols; in the results section, we will only refer to their absolute values, i.e., $A = |\tilde{A}|$ and so on, as we do not evaluate the phase angles of the coefficients. Note that the symmetry coefficients consist of different sets of susceptibility tensor elements and that for each of the four light polarization combinations (pp, ps, sp, ss) these sets are different; details of the derivation of eq 1 and a review of SHG anisotropy measurements can be found in ref 14. All measurements presented here were done in pp configuration.

It was shown that, due to third-order nonlinear effects, the isotropic contribution to the SH signal contains a term proportional to the normal component of the interfacial electrostatic field E^{DC} in the double layer[9]

$$\tilde{A} = \tilde{A}^{(2)} + \tilde{A}^{(3)}E^{DC} \tag{2}$$

where $\tilde{A}^{(2)}$ and $\tilde{A}^{(3)}$ represent the second and third-order sources of the isotropic term. The interfacial field, in turn, depends on the surface charge density on the metal σ_M

$$E^{DC} = \frac{4\pi\sigma_M}{\epsilon_0\epsilon_{DL}} \tag{3}$$

with the dielectric function of the double layer ϵ_{DL} coming in as a parameter that may not be a constant as the electrode potential is varied. Thus, by measuring the rotational anisotropy of the SH signal from the Au electrode and analyzing it with respect to its isotropic (*A*) and anisotropic (*B*, *C*, *D*) symmetry contributions, we obtain in situ information on adsorption processes as well as changes in the surface structure during electrochemical processes.

The electrochemical cell was specifically designed to permit optical SHG and cyclic voltammetry (CV) measurements in the hanging meniscus configuration to be performed simultaneously; details are published elsewhere.[9,15] It consisted mainly of a Kel-F compartment with an optical window at the bottom, see Figure 1b. Immediately after the crystal has been inserted into the cell, the electrolyte solution and the cell setup is purged with argon (5.0) to protect the sample surface from contamination and to clean the electrolyte and cell from air.

For the optical SHG measurements, a Nd:YAG laser was used that provides 5 ns pulses with ~100 mJ per pulse at a repetition rate of up to 10 Hz and a fundamental wavelength of 1064 nm. The laser light was directed upward into the cell by means of a prism and reflected off the sample hanging face-down in contact with the electrolyte solution; see Figure 1b. Behind the cell, the fundamental beam was blocked by a filter, and the SHG intensity was recorded using a photomultiplier tube. The sample could be rotated around its surface normal using a step-motor; this way, the rotational anisotropy of the SH signal could be measured.

For electrochemical experiments, the cell was equipped with a Pt ring wire as a counter electrode and a salt-bridged reference electrode compartment. A potentiostat offering an analog voltage ramp was used to obtain the CV data.

The conventional way to measure the SHG anisotropy is to set the potential to a desired value, then rotate the sample in, e.g., 5° steps until a full rotation of the surface around its normal is completed and measure the SH intensity at each angular position. To obtain better data quality, the rotation is repeated several times before setting the electrode potential to a new value. The resulting anisotropy curve is fitted using eq 1 or Fourier-analyzed to yield the symmetry components *A*, *B*, *C*, and *D*. The advantage of this technique is the high degree of determination of the fit or Fourier analysis, since every curve is defined by, in this case, 72 points.

On the other hand, in this procedure static potentials are applied to the electrode for the time of the anisotropy measurement; a full potential cycle is completed very slowly. Simultaneous voltammetric control of the current response is impossible. In systems that are dominated by reaction currents, the electrochemical parameters in general do not stay constant over a long time. Thus, the SHG results are very difficult to reproduce and correlate to cyclic voltammetry (CV) results obtained in a separate experiment. Consequently, a different technique was developed, where the rotational position of the sample was set to a desired angle and the SH intensity was recorded together with the electrode current during a conventional potential sweep. This was repeated for all anisotropy minimum and maximum positions, resulting in 12 intensity scans. From eq 1 it can be calculated that

$$\frac{1}{6_{min}}\sum I_{SHG}(\varphi, U_{el}) = A_r^2 + A_i^2 + \frac{1}{2}(B_r^2 + B_i^2 + C_r^2 + C_i^2) \tag{4}$$

and

$$\frac{1}{6_{max}}\sum I_{SHG}(\varphi, U_{el}) = A_r^2 + A_i^2 + \frac{1}{2}(B_r^2 + B_i^2 + C_r^2 + C_i^2 + D_r^2 + D_i^2) \tag{5}$$

where the indices r and i denote the real and imaginary parts of the coefficients, respectively. Taking into account that on well-prepared fcc-(111) surfaces $B, C \ll A, D$, eq 4 yields to a good approximation

$$\sqrt{\frac{1}{6_{min}}\sum I_{SHG}(\varphi, U_{el})} \simeq |A(U_{el})| \tag{6}$$

whereas the difference of eqs 4 and 5 yields

$$\frac{1}{6_{max}}\sum I_{SHG}(\varphi, U_{el}) - \frac{1}{6_{Min}}\sum I_{SHG}(\varphi, U_{el}) = \frac{1}{2}|D(U_{el})|^2 \tag{7}$$

Hence the specialty of this method is that the scan mode data can be used to obtain the isotropic (*A*) and 3-fold contribution (*D*). As the time base for these data is the same as for CV, direct correlation of the SHG results with the current response of the system is possible.

3. Results and Discussion

3.1. Camphor in Perchlorate Base Electrolyte. $NaClO_4$ without Camphor. The nonlinear optical response of Au(111) surfaces, in particular the behavior of the isotropic and anisotropic components as a function of applied electrode potential, is dominated by two processes, namely the formation and lifting of surface reconstruction and the surface oxidation.[16,17] The formation of a $(\sqrt{3} \times 23)$ reconstructed surface in principle produces one- and 2-fold contributions to the SH anisotropy. Because of the equivalence of the three $[\bar{1}10]$ directions, however, the distinct field sources cancel out.

On the other hand, the surface reconstruction decreases the 3-fold symmetry of the surface, resulting in a drop of the 3-fold term *D* of the SHG anisotropy:

$$D\cos 3\phi \rightarrow D_{rec}\cos 3\phi \tag{8}$$

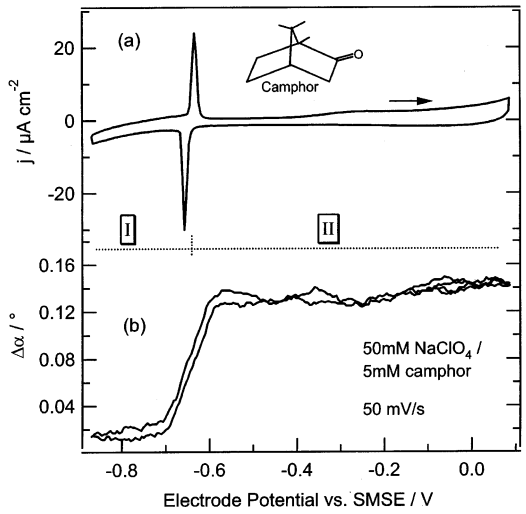

Figure 2. Au(111) thin film electrode in 50 mM $NaClO_4$ + 5 mM camphor. (a) CV taken at 50 mV/s. (b) Surface plasmon resonance angle shift measured simultaneously with CV. Regions I and II: see text.

The 3-fold term is generally a sum of four elements of the second-order susceptibility tensor:

$$D = \frac{1}{4}(\chi_{xxx} - \chi_{xyy} - 2\chi_{yxy}) \tag{9}$$

with $\chi_{yxy} = \chi_{yyx}$. On an ideal, nonreconstructed fcc-(111) surface $\chi_{xyy} = \chi_{yxy} = -\chi_{xxx}$ and thus $D = \chi_{xxx}$. For the reconstructed surface we have $\chi_{xyy} \neq -\chi_{xxx}$ and $\chi_{yxy} \neq -\chi_{xxx}$. Assuming that the two off-diagonal elements are changed by reconstruction by approximately the same amount, such that

$$\chi_{xyy} = \chi_{yxy} = -r\chi_{xxx} \tag{10}$$

where $r \leq 1$ is a parameter describing the reconstruction-induced change of the susceptibility, we obtain

$$D_{\mathrm{rec}} = D\frac{1}{4}(1 + 3r) \tag{11}$$

Indeed, in SHG measurements on Au(111) in $NaClO_4$ electrolyte, a gradual increase of the 3-fold term D upon lifting of the reconstruction in the positive potential sweep was observed.[9] The change in D was approximately 25%, corresponding to a variation in r from 1 in the case of a (1×1) surface to $r = 0.66$ for the reconstructed surface.

$NaClO_4$ Containing 5 mM Camphor. The voltammetric and SPR responses of a Au(111) film electrode in 50 mM $NaClO_4$ with 5 mM camphor at a scan rate of 50 mV/s can be seen in Figure 2. The pronounced current peak separating regions I and II in Figure 2a indicates the phase transition in which from a gaslike phase (I) a 2D-condensed camphor phase is formed (II). The current peak is caused by a rapid change of the double layer capacity during the camphor phase transition. The SPR shift plotted in Figure 2b shows a marked step at the transition from region I to region II and back. This is due to camphor molecules forming a dense coverage on the Au surface thus inducing a substantial change in the surface dielectric function. Within each region, the surface plasmon resonance angle is nearly invariant with respect to potential variations.

The SHG of a Au(111) surface in 0.1 M $NaClO_4$ containing 5 mM camphor has been investigated and is reported in detail in ref 9. In Figure 3, the 3-fold terms of Au(111) in 0.1 M $NaClO_4$ without and with 5 mM camphor (a) are plotted together

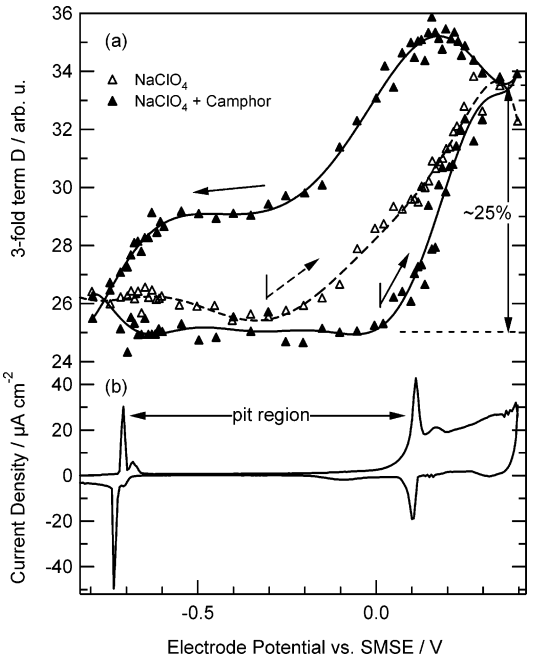

Figure 3. Au(111) single-crystal electrode in 0.1 M $NaClO_4$ + 5 mM camphor. (a) SHG 3-fold term D obtained from anisotropy curves taken at consecutive potentials. The sample was immersed at −0.8 V, where the measurement cycle starts. Open symbols: measured in perchlorate solution without camphor. Full symbols: data in perchlorate solution with camphor. (b) For comparison, a CV taken in 0.1 M $NaClO_4$ + 5 mM camphor at 10 mV/s.

with a typical current−voltage diagram of the camphor-containing electrolyte (b). As a larger potential range compared to Figure 2 is displayed, a second current peak at a more positive potential is apparent, indicating another phase transition. The potential region between the two phase transitions is characterized by a nearly constant, low capacity ("pit region") and lies entirely outside the oxidation potentials of Au(111). The SHG data presented in this figure was obtained using the "anisotropy mode", i.e., recording a full rotational anisotropy curve at constant potential and then changing the potential; this method yields low variance in the data but imposes rather long measurement times.

It can be seen that while in pure perchlorate electrolyte the 3-fold term starts rising approximately at −300 mV (SMSE) due to the lifting of the reconstruction, the surface structure remains unchanged in the presence of camphor. Only as the second phase transition occurs (around 100 mV) is the reconstruction lifted. Thus, it can be seen that the 2D-condensed layer stabilizes the reconstructed surface up to the point where the 2D camphor layer undergoes a second discontinuous transition. On the potential scan in negative direction, the data show that the reconstruction is partially rebuilt between +200 and −200 mV, while between this potential and approximately −700 mV, at which point camphor leaves the surface, the surface structure is unchanged. In this regime, camphor suppresses further formation of the surface reconstruction. This leads to the coexistence of reconstructed and (1×1) domains, which causes a splitting of the phase transition peaks at the negative end of the potential range.[7,8,9]

3.2. Periodate in Perchlorate Base Electrolyte. Next we consider the reduction reaction of periodate ions IO_4^- in 0.1 M $NaClO_4$ base electrolyte. Figure 4a shows the cyclic voltammogram of 5 mM $NaIO_4$ in 100 mM $NaClO_4$ taken at 50 mV/s. The complete CV is dominated here by Faradaic currents; as electrons are transferred from the electrode into the oxidized

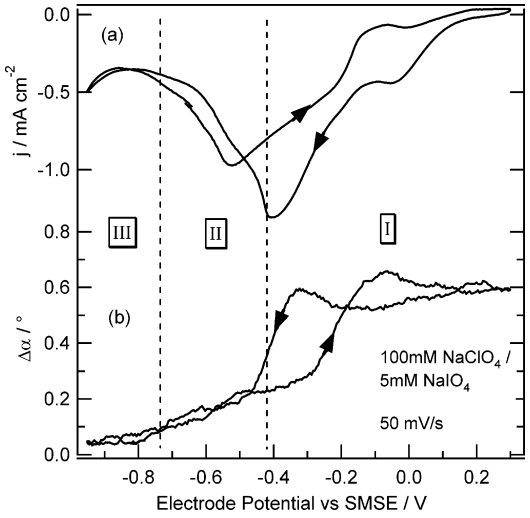

Figure 4. CV (a) and SPR shift (b) of Au(111) film electrode in 0.1 M $NaClO_4$ + 5 mM $NaIO_4$ taken at 50 mV/s. Regions: I, anion covered state of the electrode; II, NDR regime; III, low reaction current. For further discussion of regions, see text.

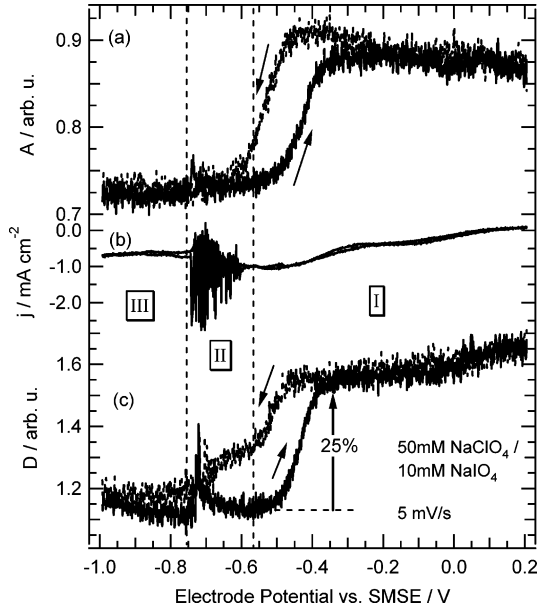

Figure 5. SHG isotropic term *A* (a), CV (b), and SHG 3-fold term *D* (c) of a Au(111) single-crystal electrode in 50 mM $NaClO_4$ + 10 mM $NaIO_4$. SHG data are taken in the scan mode, simultaneously with the current, at a scan rate of 5 mV/s. Regions I, II, and III: see Figure 4 and text.

species, the reaction rate increases as the potential is made more negative in region I. In region II, the reaction rate—and therefore the current—drops, while the driving force of the reaction continues growing; this results in a negative differential resistance (NDR). At the negative end of the potential range (region III), a somewhat decreased but approximately steady reaction current can be seen.

In Figure 4b the SPR shift, recorded simultaneously with the CV in panel a is shown. It displays a clear downward step in the negative scan direction around −0.4 V indicating the desorption of periodate-derived anions from the electrode surface; in the positive scan direction, the upward step around −0.2 V signifies the ion adsorption. The reduction reaction of periodate in aqueous electrolyte is

$$IO_4^- + H_2O + 2e^- \rightarrow IO_3^- + 2OH^- \qquad (12)$$

whose normal potential is given as 0.68 V (NHE),[18] i.e., 0.03 V vs SMSE. Details of the reaction mechanism however remain unclear, particularly in view of the interplay between adsorption and the occurrence of a NDR regime; these questions are not in the scope of the present publication.

Two remarkable features of the adsorption process should be noted here: first, by comparing the current response with the SPR data, it becomes evident that there is no simple correlation between anion adsorption and desorption and the reaction current. This shows the complexity of the reaction process, as on one hand, the adsorbed species must play a role in the reaction but on the other hand the reaction rate seems independent of the coverage. Second, the SPR data in Figure 4b show that the NDR region lies in the potential range of the desorbed state. As can be seen in the negative scan, the differential resistance becomes negative when most of the anions are desorbed. The implications of this behavior in view of the electrode dynamics leading to a negative differential resistance are to be further investigated.

Because of reaction currents dominating the full potential range, the scanning-mode SHG-anisotropy method was chosen to obtain the rotational symmetry coefficients of this system. SHG measurements were performed on Au(111) in 50 mM $NaClO_4$ containing 10 mM $NaIO_4$. Typical representations for the isotropic term *A* and the 3-fold term *D*, calculated from scan mode measurements as described above, are shown together with a current−voltage curve in Figure 5. It can be seen in panel b that, here, the NDR region (II) is characterized by strong current oscillations that arise from the interplay of the NDR with the ohmic potential drop $U_{el} = IR_{el}$ across the electrolyte solution. The oscillations develop in this system due to the lower electrolyte conductivity compared to that in Figure 4.

In Figure 5a, a distinct step in the isotropic term around −0.43 V (positive direction of potential sweep) and −0.54 V (negative direction) can be seen. This indicates a change in the interfacial field due to specific adsorption of a periodate species. Only two states of the electrode can be distinguished throughout the potential range: as the adsorbed species is anionic, the upper branch between −0.35 and 0.2 V represents the adsorbed state, whereas below −0.6 V, the surface is in the desorbed state.

In Figure 5c, the development of the 3-fold symmetry term *D* during a potential cycle is shown. On the positive-going scan, an increase of around 25% of the maximum value coincides with anionic adsorption. For potentials more positive than −0.35 V, i.e., in the adsorbed state, *D* does not change significantly any more. Since it is well-known that specific adsorption of anions such as halide ions lifts the reconstruction of Au(111),[19−22] we conclude that here the same effect occurs. This is supported by the observation that, again, the change in *D* amounts to ∼25%, characteristic for the lifting and formation of the $(\sqrt{3} \times 23)$ reconstruction of Au(111). On the potential sweep in the negative direction, the 3-fold symmetry term *D* exhibits a deviation from the behavior of the adsorption as reflected by the *A*-term. The data show that from −0.48 V toward more negative potentials, *D* first drops in parallel with the *A*-term. However, when the *A*-term has reached its final value, the *D*-term continues decreasing and saturates only at −0.8 V. This indicates that the rate at which the reconstruction forms is slower than the rates of desorption, adsorption and lifting of the reconstruction.

The *A*- and *D*-data exhibit a further remarkable feature: they oscillate together with the current in the negative range of region II. The oscillations are necessarily poorly resolved as the *A*-

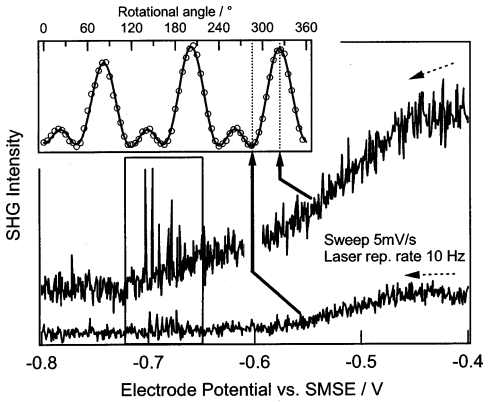

Figure 6. Au(111) in 50 mM $NaClO_4$ + 10 mM $NaIO_4$; SHG intensity at two representative rotational angles as a function of potential during cathodic (as indicated by dashed arrows) potential sweeps at 5 mV/s. The laser repetition rate was 10 pulses per second. The inset shows the full rotational anisotropy curve taken with the electrode at −0.9 V vs SMSE. The rotational positions of the SHG scans are indicated by dotted lines. The frame highlights the oscillation region around −0.69 V; oscillations are visible both in minimum and maximum positions of the anisotropy.

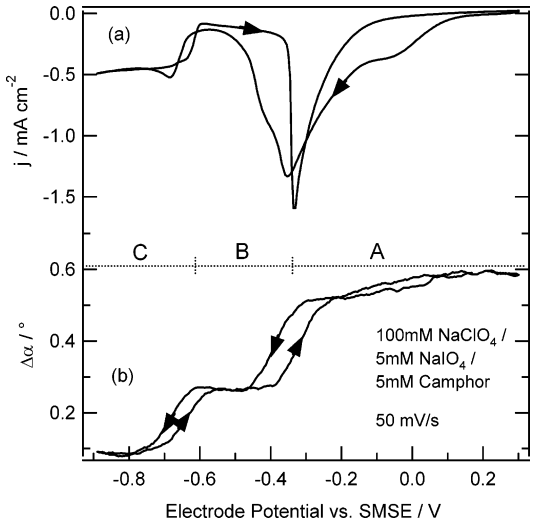

Figure 7. CV (a) and SPR shift (b) of Au(111) film electrode in 0.1 M $NaClO_4$ + 5 mM $NaIO_4$ + 5 mM camphor taken at 50 mV/s. Regions: A, anion covered state, high reaction current; B, inhibition region; C, low reaction current. For further discussion of regions, see text.

and *D*-curves shown are calculated from the sum of 6 and 12 individual potential cycles, respectively, leading to considerable averaging. However, in Figure 6, raw SHG intensity traces providing the information for calculating *A* and *D* are plotted for two representative rotational angle positions, namely a minimum and a maximum, as depicted in the inset. The potential is swept at a rate of 5 mV/s, the laser repetition rate is 10 pulses per second. The oscillations, whose frequency changes as a function of potential from below to well above 10 Hz, are not well resolved yet are clearly visible in the SHG measurements. The SHG data reveal oscillations at all rotational angles, suggesting that the current oscillations are accompanied by oscillations in the anion coverage as well as in the degree of reconstruction.

Periodic changes of the periodate-derived adsorbate coverage were confirmed by SPR measurements[10] as well as by measurements of the SHG intensity at the angular position at which the anisotropy has a minimum. Both quantities are dominated by the coverage of the electrode with adsorbates (cf. Figures 4 and 5); thus their oscillations prove that the coverage of the electrode oscillates as well. Furthermore, since in the case of large currents the cell voltage comprises both the double layer potential drop and the ohmic voltage drop through the electrolyte $U_{el} = IR_{el}$, the applied voltage can be corrected for the IR_{el}-drop; doing so, it becomes evident that in the oscillations with larger amplitudes the double layer potential ϕ_{DL} changes between potentials where the electrode is adsorbate free and more positive potentials at which a species is adsorbed.

The oscillations seen in the *D*-term suggest that the oscillations also imply partial lifting and re-formation of the reconstruction. Only if *D* was partially influenced by the adsorption of the anions would this statement not be conclusive. However, there are two observations which strongly support the assumption that the contribution of adsorbed species to the *D*-term is negligible. First, as mentioned above, the change in *D* amounts to 25%, and this value is in perfect agreement with the value measured for the transition between reconstructed and unreconstructed Au(111) surfaces in different electrolytes.[9] Second, a change of the *D*-term induced by an adsorbed species could only be due to chemisorption, which would decrease the density of free surface electrons through bond formation. Consequently, it should lead to a decrease in *D*, as indeed observed for Cl^- adsorbing on Au.[14,22] In contrast, in our case we observed an increase in the *D*-term, characteristic for the lifting of the reconstruction.

Summarizing, SPR data and the isotropic term of the SHG response evidence adsorption of anionic periodate species at the Au(111) surface. In addition, the SHG *D*-term reveals that the adsorption leads to the lifting of the reconstruction which occurs on the time scale of the adsorption. In contrast, the re-formation of the ($\sqrt{3} \times 23$) phase occurs on a slower time scale than desorption of the anions. We will now turn to the mixed system including periodate ions and camphor molecules in the same base electrolyte, studying the influence of camphor on the effects observed in the system containing only periodate.

3.3. Camphor and Periodate in $NaClO_4$. A prototypical current−voltage characteristic of Au(111) in 100 mM $NaClO_4$ containing 5 mM $NaIO_4$ and 5 mM camphor is plotted in Figure 7a. Again, an increasing reaction rate is evident as the potential is swept from positive to more negative potentials between −0.1 and −0.3 V (region A). At about −0.35 V, however, the reaction current strongly decreases and remains very small (region B) until the potential enters region C, where the current rises again to an approximately constant level. The reverse scan exhibits the same characteristics; i.e., the transition from region C to region B is accompanied by a considerable drop in current density, and crossing from region B to A, the current increases sharply. Comparing this CV to the one obtained without camphor in Figure 4a, it is apparent that the behavior in regions A and C in Figure 7a corresponds to that of regions I and III in Figure 4a, whereas in the camphor-containing system the current in region B is considerably smaller than in region II without camphor. This suggests that camphor adsorbs on the electrode and inhibits the reduction of periodate in region B. This interpretation is supported by the SPR data displayed in Figure 7b. Three surface states can be clearly distinguished, which with the help of Figures 2b and 4b can be assigned to the bare Au surface (region C), the 2D-condensed camphor-film covered surface (region B), and the periodate-derived anion-covered surface (region A). Hence, during the transition from region A to region B, the periodate-derived species is displaced by the 2D-condensed camphor film.

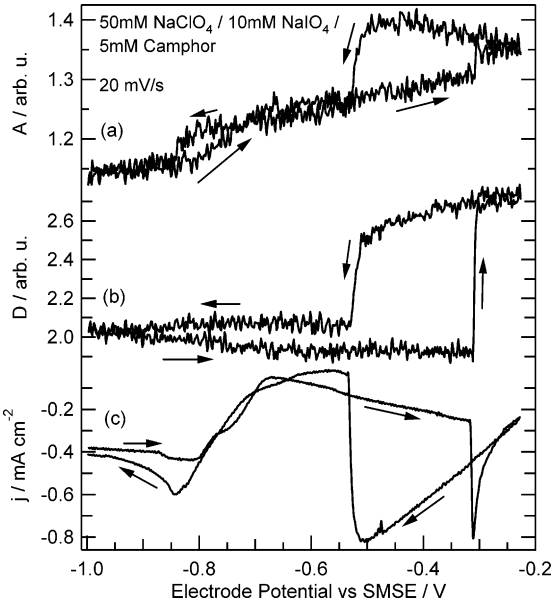

Figure 8. Au(111) single-crystal electrode in 50 mM $NaClO_4$ + 10 mM $NaIO_4$ + 5 mM camphor taken at 20 mV/s: (a) SHG isotropic term *A*; (b) SHG 3-fold term *D*; (c) cyclic voltammogram. SHG data were obtained in the scanning mode.

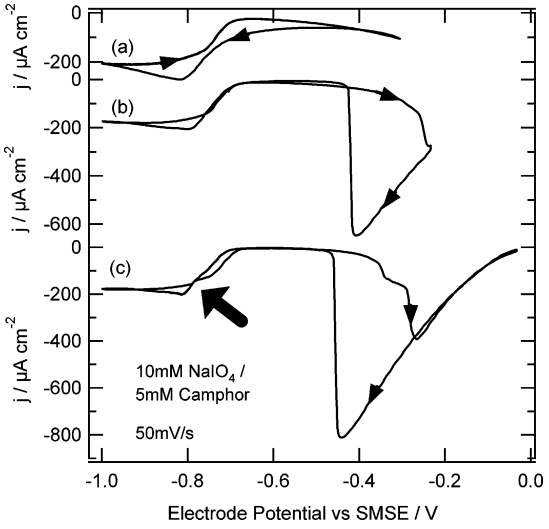

Figure 9. Cyclic voltammograms of Au(111) single-crystal electrode in 10 mM $NaIO_4$ + 5 mM camphor taken at 50 mV/s. Anodic turning potentials: (a) −0.3, (b) −0.23, and (c) −0.03 V. Thick arrow shows the double step feature in current on positive-going scan during camphor adsorption.

The concept of a replacement process between inert camphor and reacting periodate-derived anions can be confirmed by investigating the adsorption behavior of the Au(111) surface using SHG measurements. Figure 8 shows scan mode data for the SHG isotropic term *A* (a) and the 3-fold term *D* (b), together with the corresponding CV (c). The isotropic term *A* reveals the evolution of the interfacial electrostatic field as a function of the electrode potential. In close correlation with the results from SPR shift measurements seen in Figure 7, three states can be distinguished: a free-electrode state at very negative potentials ($U < -0.8$ V), a camphor-state at intermediate potentials (positive scan direction: -0.7 V $< U < -0.3$ V) and a chemisorbed ions state at the positive end of the range.

The behavior of the 3-fold term *D* on the other hand, seen in Figure 8b, indicates structural changes of the Au(111) surface during the complex processes discussed above. Starting the positive-going potential sweep at very negative potentials, where the reconstruction is stable, only a minor reduction in *D* occurs as camphor adsorbs on the surface. This is in accordance with results in a pure camphor system without periodate present.[9] Essentially, the surface reconstruction remains unperturbed in the camphor-covered region, i.e., between −0.7 and −0.3 V.

At this point (−0.31 V), concomitant with the displacement of camphor by IO_4^--derived ions and the restart of the reduction reaction, a very sharp step in *D* can be seen, the change being ca. 25% of the upper value. According to the arguments given above, this strongly indicates that the reconstruction is lifted due to anion adsorption. The lifting of the reconstruction occurs in less than 100 ms, which is much faster than in pure base electrolyte without specifically adsorbing ions present (Figure 3a, open symbols), or even compared to Au(111) in $NaClO_4$ with periodate (Figure 5). At first glance, this points to an enhancement of the lifting of the reconstruction by specifically adsorbing ions. However, one should be aware that during the transition, the current strongly increases causing a nonnegligible *IR*-drop in the electrolyte. As a consequence, the electrode potential becomes more positive during the transition thereby increasing the driving force for the formation of the (1 × 1)-phase, which also contributes to the speed of the process. In the negative scan direction, it is apparent from *A* and the current density in Figure 8, parts a and c, that camphor adsorbs on the surface at a potential where the desorption of periodate in the absence of camphor has already started; see Figure 5a. As this occurs at rather negative potentials (approximately −0.5 V), the driving force for the formation of the reconstruction is high, leading to a beginning reconstruction of the surface. In contrast to the pure periodate system characterized in Figure 5 however, camphor appears to accelerate the anion desorption and with it the formation of surface reconstruction. Again, with decreasing current during the displacement of the anions, the double layer potential abruptly becomes even more negative, further increasing the driving force for reconstruction. Nevertheless, the reconstruction is not complete, as seen from the fact that immediately after the reformation of the reconstruction, i.e., at −0.6 V, *D* fails to resume the value of the positive scan direction. This is confirmed by the fact that if the potential sweep is reversed at a potential negative of −0.31 V (data not shown), the gap in *D*(positive direction) − *D*(negative direction) does not occur. Obviously, during the ion-camphor exchange, the surface is rapidly reconstructed, until camphor reaches a complete coverage and suppresses further reconstruction.

The fact that the reconstruction is not completely rebuilt leads to a double-step behavior of the current during camphor adsorption.[8,9] In Figure 8c on the positive-going potential scan, the current drops from approximately −0.45 mA/cm^2 at −0.8 V first to −0.3 mA/cm^2 at −0.75 V and then to −0.05 mA/cm^2 at −0.67 V. This behavior is only seen if the potential is swept more positive than −0.3 V, where the anion adsorption takes place. Figure 9 shows a more detailed voltammetric analysis of the effect. In Figure 9a a current−potential curve can be seen, taken with a Au(111) crystal immersed in 10 mM $NaIO_4$ containing 5 mM camphor. The adsorption and desorption of camphor leads to a smooth decrease and increase of the reaction current, respectively, between −0.82 and −0.66 V. As the anodic reversal potential is set more positive, cf. Figure 9b, the anodic scan shows a current increase at −0.25 V due to the replacement of camphor by periodate-derived anions, similar to Figure 8c; the camphor adsorption region around −0.75 V remains essentially unchanged. Only after choosing an even more positive anodic turning point does the double-step current

response during camphor adsorption occur; see arrow in Figure 9c. A change in the camphor adsorption is induced by sweeping the potential beyond −0.24 V and moving the potential positive enough, which also means keeping the electrode positive of the camphor/periodate exchange potential for long enough.

In the system without periodate, the camphor condensation is split into two distinct peaks in case the potential has been swept past the anodic camphor phase transition, compare Figure 3b; hence, we conclude that here, too, the camphor adsorption around −0.75 V is split into two steps due to unreconstructed domains remaining on the surface after lifting the reconstruction and re-forming it on most parts of the surface area. The SHG data in Figure 8b show that the reconstruction is rapidly lifted during the adsorption of periodate-like anions. However, the double step does not occur in Figure 9b, where the anion adsorption has taken place (and thus the reconstruction has been lifted) but the anodic reversal potential is only some mV positive of this point. Contrary to that, the double step is visible when the reversal point is well positive of the camphor-ion exchange point at −0.24 V. Evidently, despite the reconstruction being lifted within milliseconds, the formation of unreconstructed domains on the negative potential sweep depends on a process occurring on a much larger time scale.

It is known that as the $(\sqrt{3} \times 23)$-reconstruction of Au(111) is electrochemically lifted, the surface contraction relaxes and the excess material is deposited on the crystal face in the form on monatomic islands. The islands are subject to Ostwald ripening if the potential stays in the regime where the (1×1) structure is stable.[23,24] The growth of islands due to ripening depends on the surface adatom diffusion constant and will occur on the time scale of seconds. From the observation that unreconstructed domains develop only if the reconstruction has been lifted long enough in sufficiently positive potentials, we deduce that the growth and stability of the islands plays a crucial role in the formation of the reconstruction. In the case shown in Figure 9b, the potential sweep is reversed before islands can form and grow significantly, leaving excess Au atoms diffusing freely on the surface; therefore the reformation of the reconstruction is complete and uniform throughout the surface area. In Figure 9c however, after lifting the reconstruction the islands have been allowed to grow and stabilize; as a consequence, the formation of reconstruction on the reversed scan is slowed in some parts of the surface, while others reconstruct normally. The formation of a condensed camphor layer on the negative scan comes in as a further complication: it will "freeze" any further surface restructuring before it is complete, as observed in the pure camphor system displayed in Figure 3. Thus, the reconstruction is incomplete on the negative scan if, in the positive direction, the potential has been cycled sufficiently positive of the lifting potential.

This picture is confirmed by earlier STM studies.[25] There, with Au(111) in perchloric acid, the potential was pulsed from a value where the reconstruction is stable to a more positive potential where the (1×1) structure is stable, and back. After applying the pulse, the temporal evolution of the islands was imaged. The authors found that the longer and more positive the pulse was, the longer the islands persisted at negative potentials (up to >100 s!) and the longer it took for the atoms to be incorporated in domains of $(\sqrt{3} \times 23)$ reconstruction. During the pulse, the authors conclude, on the time scale of several seconds (compliant with our observations) a "voltammetric annealing" stabilizes the islands, thus slowing down the re-formation of the reconstruction.

4. Conclusions

We used a combination of SHG anisotropy measurements, SPR shift measurements and cyclic voltammetry to investigate the behavior of a Au(111) single crystal surface under the influence of camphor and periodate added to the base electrolyte. Conventional SH anisotropy measurements (recording every anisotropy curve at constant potential) are suited only for nonreactive systems, where the electrochemical properties are not likely to change when static potentials are applied over a longer period of time. Here, however, a different approach was followed; the SH intensity at several fixed angular positions was recorded during a potential sweep used at the same time for cyclic voltammetry. The SHG isotropic and 3-fold terms were obtained from these data. This technique makes it possible to relate the nonlinear optical response of the electrode surface directly to the current, as both are measured on the same time base. Information on adsorption and adsorbate phase transitions was drawn from SPR measurements; measurement of the isotropic contribution A to the SHG signal supplemented and confirmed these results. Structural parameters of the surface during electrochemical processes could be followed in the anisotropic contributions to SHG. In particular, it was shown that the formation and lifting of surface reconstruction can be monitored in the 3-fold term D, even under reaction conditions and in the presence of different adsorbates.

We have shown that for Au(111) immersed in neutral 0.1 M $NaClO_4$ electrolyte containing 5 mM camphor, a 2D condensed layer of camphor molecules is formed which stabilizes the reconstructed surface to ∼0.3 V more positive potentials than without camphor. On the cathodic scan, the same layer partially suppresses the electrochemical reformation of the reconstruction leading to nonreconstructed domains prevailing on the surface.

Periodate, on the other hand, added to the base electrolyte as 10 mM $NaIO_4$, is reduced to IO_3^- at negative potentials on Au(111). In this reaction, adsorbed periodate-derived anions play an important role which is to be unveiled in further experiments. Combined SHG and SPR results allow for unambiguous distinction between adsorbed and nonadsorbed states of the electrode surface. Between −0.6 V and −0.8 V, the system exhibits a negative differential resistance that, depending on the base electrolytic resistivity, can lead to current oscillations. It could now be shown that, during these oscillations, the electrode rapidly alternates between the adsorbed and free states. Regarding the gold surface structure, it was found here that the anion adsorption leads to a more rapid lifting of the surface reconstruction and that during the current oscillations, parts of the surface area periodically switch between $(\sqrt{3} \times 23)$ and (1×1).

If camphor is added to the periodate reduction system, the reaction is efficiently inhibited in an intermediate potential region, where camphor forms a condensed molecular layer on the surface. Our results show that negative of the inhibition region, the surface is free of adsorbates, whereas toward more positive potentials, camphor is replaced by periodate-like anions adsorbing at the surface; at this point, the periodate electroreduction is resumed. Concomitant with this, the surface reconstruction is rapidly lifted due to the adsorption of ions and the abrupt change in the double layer potential during the steep current increase. Our results show that after the transition to (1×1) in the positive scan direction, Au islands grow and stabilize, the more positive the potential gets. If the potential is cycled sufficiently far beyond of the $(\sqrt{3} \times 23) \rightarrow (1 \times 1)$ transition (for a sufficiently long time), the formation of the reconstruction on the cathodic half-cycle will be hindered due to slow dissolution of the islands. Therefore, the reconstruction

is not completely rebuilt. Reconstructed and (1 × 1) domains coexist on the surface.

Both SPR and SHG proved robust against Faradaic processes which dominate the current−voltage characteristic and make it difficult to resolve, e.g., the lifting of the reconstruction or the camphor phase transition from CV alone. Thus, the combination of SHG, SPR, and CV used here is particularly promising for further investigations of reactive systems due to the complementarity of the methods, where CV yields more dynamic and reaction information, while SPR and SHG probe electrostatic, adsorbate, and structural effects, independent of the reaction.

References and Notes

(1) Li, Y. J.; Oslonovitch, J.; Mazouz, N.; Plenge, F.; Krischer, K.; Ertl, G. *Science* **2001**, *291*, 2395.

(2) Stolberg, L.; Lipkowski, J. *Adsorption of organic molecules at metal electrodes*; Lipkowski, J., Ross, P., Eds.; VCH: New York, 1992; Chapter 4.

(3) Lust, E.; Jänes, A.; Miidla, P.; Lust, K. *J. Electroanal. Chem.* **1997**, *425*, 25.

(4) Bare, S.; van Krieken, M.; Buess-Herman, C.; Hamelin, A. *J. Electroanal. Chem.* **1998**, *445*, 7.

(5) Van Krieken, M.; Buess-Herman, C. *Electrochim. Acta* **1998**, *43*, 2831.

(6) Dretschkow, Th.; Wandlowski, Th. *Electrochim. Acta* **1998**, *43*, 2991.

(7) Striegler, H. Ph.D. Thesis, Universität Ulm, 1998.

(8) Striegler, H.; Krznaric, D.; Kolb, D. M. *J. Electroanal. Chem.* **2002**, *532*, 227.

(9) Pettinger, B.; Danckwerts, M.; Krischer, K. *Faraday Discuss.* **2002**, *121*, 153.

(10) Li, Y. J. Ph.D. Thesis, FU Berlin, Berlin 2003; www.diss.fu-berlin.de/2003/73.

(11) Plenge, F.; Li, Y.-J.; Krischer, K. *J. Phys. Chem. B* **2004**, *108*, 0000.

(12) Hamann, C.; Vielstich, W. *Elektrochemie*; Wiley-VCH: Weinheim, Germany, 1998.

(13) Agranovich, V. M., Mills, D. L., Eds. *Surface Polaritions: Electromagnetic Waves at Surfaces and Interfaces*; North-Holland: Amsterdam, 1982.

(14) Pettinger, B.; Bilger, C.; Lipkowski, J.; Schmickler, W. *Interfacial Electrochemistry*; Wieckowski, A., Ed.; Marcel Dekker: New York, 1999; p 373.

(15) Danckwerts, M.; Savinova, E.; Pettinger, B.; Doblhofer, K. *Appl. Phys. B: Mater. Sci. Process.* **2002**, *74*, 635.

(16) Pettinger, B.; Lipkowski, J.; Mirwald, S.; Friedrich, A. *Surf. Sci.* **1992**, *270*, 377.

(17) Pettinger, B.; Lipkowski, J.; Mirwald, S. *Electrochim. Acta* **1995**, *40*, 133.

(18) Roman, W. *Gmelins Handbuch der Anorganischen Chemie*, 8th ed.; Verlag Chemie: Berlin, 1933; Vol. 8 (Iodine), p 528.

(19) Wang, J.; Davenport, A. J.; Isaacs, H. S.; Ocko, B. M. *Science* **1992**, *255*, 1416.

(20) Ocko, B. M.; Magnussen, O. M.; Adzic, R. R.; Wang, J. X.; Shi, Z.; Lipkowski, J. *J. Electroanal. Chem.* **1994**, *376*, 35.

(21) Magnussen, O. M.; Ocko, B. M.; Wang, J. X.; Adzic, R. R. *J. Phys. Chem.* **1996**, *100*, 5500.

(22) Pettinger, B.; Bilger, C.; Lipkowski, J. Solid−Liquid Interfaces. *Topics Appl. Phys.* **2003**, *85*, 223.

(23) He, Y.; Borguet, E. *Faraday Discuss.* **2002**, *121*, 17.

(24) Icking-Konert, G. S.; Giesen, M.; Ibach, H. *Surf. Sci.* **1998**, *398*, 37.

(25) He, Y.; Borguet, E. *J. Phys. Chem. B* **2001**, *105*, 3981.